Observation and verification of the Fresnel and Arago interference laws using adaptive photodetectors

P. Rodríguez-Montero
Instituto Nacional de Astrofísica, Optica y Electrónica,
Luis Enrique Erro #1, Tonantzintla, Pue. 72840, México.

Received 24 April 2020; accepted 7 July 2020

The Fresnel and Arago interference laws relate the polarization of the electromagnetic field to the interference phenomenon. Different methods and interferometers have been reported to verify these laws; most of them rely on visual inspection to determine the positions of maximum and minimum interference. In this report, the observation and verification of the Fresnel and Arago interference laws using adaptive photodetectors are presented. These photodetectors generate an electrical current proportional to the square of the visibility of the interference pattern; thus, the gradual change from the appearance of the interference pattern (maximum visibility) to its disappearance (minimum or null visibility) is detected as an electrical current. The extreme values of the interference pattern visibility can be accurately assessed, in real time and without the need of any signal processing. A difference of 3 orders of magnitude between the electrical signals measured in the maximum and minimum intensity regions in the interference pattern is demonstrated. Due to the adaptive properties of the photodetectors (compensation of the irregularities of the interfering beams and suppression environmental fluctuations), the proposed method can be suitable for teaching purposes in undergraduate laboratories.

Keywords: Polarization; interference; adaptive photodetectors.

PACS: 42.25.Hz; 42.25.Ja; 42.25.Kb; 42.70.Nq

DOI: https://doi.org/10.31349/RevMexFisE.18.44

1. Introduction

The visibility or contrast of interference fringes produced by the superposition of two waves is strongly dependent not only on the spatial and temporal coherence of the electromagnetic field, but also of its state of polarization. The laws that relate polarization of the electromagnetic field and interference are known as Fresnel and Arago laws [1]. In modern terms, they can be stated as follows [2,3]:

1. Two waves linearly polarized in the same plane can interfere.

2. Two waves linearly polarized with perpendicular polarizations cannot interfere.

3. Two waves linearly polarized with perpendicular polarizations, if derived from perpendicular components of unpolarized light and subsequently brought into the same plane of polarization, cannot interfere.

4. Two waves linearly polarized with perpendicular polarizations, if derived from the same linearly polarized wave and subsequently brought into the same plane of polarization, can interfere.

These laws have been corroborated experimentally using different interferometers, among them, we can mention the Michelson interferometer [4], the Young interferometer [5,6], and the Mach-Zehnder interferometer [7,8]. The use of gratings as beam splitters and birefringence elements has been reported to overcome some experimental problems [9,10]. Details on the experimental difficulties and limitations of these methods are described in Ref. [6]. Analytical proofs of Fresnel and Arago laws derived for first principles have been reported in Refs. [11,12].

In the majority of the aforementioned experimental methods, only the points of maximum visibility (total interference) and minimum visibility (null interference) are reported to corroborate the Fresnel and Arago laws, and the position of these points relies mainly on visual inspection.

The following reports experimental results on the utilization of adaptive photodetectors based on the non-steady state photoelectromotive force [13,14] to verify the Fresnel and Arago interference laws. One feature of these adaptive photodetectors is that they generate an electrical current which is proportional to the square of the visibility or contrast of the interference pattern. So, the use of adaptive photodetectors allows the electrical detection of the points of total and null interference as well as the gradual changes from one position to the other as a function of the relative orientation of the linear polarization between the two interfering beams. In contrast to the previously reported detection methods, which employed CCD cameras or visual inspection, the proposed method does not need record images and perform image processing

2. Adaptive photodetectors

The adaptive photodetectors are detectors based on the non-steady-state photo-electromotive force (p-emf) effect. This effect consists in the generation of an alternating electrical current through a short-circuited photoconductive material when it is illuminated by an oscillating, spatially non-uniform

light pattern. The current is the result of the spatial mismatch between the relatively stable space-charge electric field distribution $E_{SC}(x)$, stored in the impurity centers of the photoconductive material, and the photo-excited carriers' distribution $\sigma(x,t)$, which follows the instantaneous light distribution, that is $\sigma(x,t) \propto I(x,t)$ [13,14].

To observe the effect, the photoconductive sample is usually illuminated by an oscillating interference pattern formed by two coherent plane waves, one of which is phase modulated at frequency f. For the present report, the electrical current i generated by the adaptive photodetector can be expressed as [14,15]:

$$i(V) = CAI_0V^2K(\alpha)F(f), \tag{1}$$

where A is the amplitude of the phase modulation, I_0 is the average intensity impinging on the adaptive photodetector, V is the visibility of the interference pattern, $K(\alpha)$ and $F(f)$ are functions that depend on the spatial frequency of the interference pattern and the phase modulation frequency, respectively, α is the interference angle between the two beams, and the constant C groups several electroptical constants. The visibility of the interferece pattern is given by [16,17]:

$$V = \frac{2\sqrt{I_1 I_2}}{I_0}|\gamma|, \tag{2}$$

where I_1 and I_2 are the intensities of the interfering beams at the adaptive photodetector, $I_0 = I_1 + I_2$, and γ is the complex degree of coherence.

These detectors have been named adaptive photodetectors in the sense that they can detect very efficiently high-frequency, low-amplitude phase modulated signals in the presence of low-frequency, high-amplitude phase shifts (such as those produced by environmental perturbations) and can produce an efficient signal with interfering beams with irregular wavefronts (even the ones modulated with speckle). These features are the result of the dynamic properties on the formation of the space charge electric field E_{SC} and the holographic processes involved in the formation of the p-emf electrical current [13,14]. As detectors of phase modulated signals, the theoretical sensitivity of adaptive photodetectors, that is, the minimal detected amplitude of phase modulation is $\cong 2 \times 10^{-7}$ rad($\sqrt{\text{mW/Hz}}$) (or 134 dB$\sqrt{\text{Hz/mW}}$), which is about 1 order of magnitude worse than the theoretical estimate for an ideal photodiode [18]. On the other hand, compared to solar cells, they present a very low light-to-current conversion efficiency; at room temperature and in the visible range, the theoretical efficiency for the adaptive photodetectors is about $\approx 3 \times 10^{-4}$ [13,18]. Adaptive photodetectors have been employed for measuring the coherence length of light sources [17], for detecting small amplitude vibrations, such as those produced by laser-generated ultrasonic displacements in rough surfaces [19], for characterization of femtosecond pulses [20], and for monitoring cardiac activity [21].

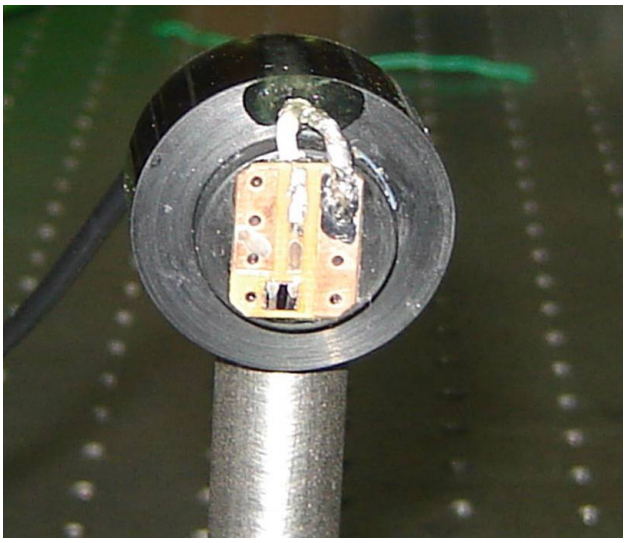

FIGURE 1. Photograph of the adaptive photodetector employed.

Figure 1 shows a photograph of the actual adaptive photodetector we used in this report. It was fabricated from a piece of GaAs:Cr crystal with approximate dimensions of $3.2 \times 3.2 \times 0.5$ mm, glued to a printed circuit board. Two parallel electrodes were deposited on its front surface (3.2×3.2 mm) with silver paint, in such a way that the effective interelectrode dimensions were $L_x \cong 1$ mm (horizontal) and $L_y = 3.2$ mm (vertical). Finally, with 20 μm gold wires the silver painted electrodes were connected to a coaxial cable.

3. Experimental setup

The experimental setup to observe the Fresnel and Arago interference laws using an adaptive photodetector is depicted in Fig. 2. A 3 mW randomly polarized He-Ne with a emission wavelength of $\lambda = 632.8$ nm laser is divided in two beams by a broadband non-polarizing beamsplitter. A phase modulation of amplitude A at frequency f is introduced in one of the beams (named beam 1) after it is reflected from a mirror glued to a vibrating piezoelectric transducer driven by a signal generator. This phase modulated beam is superimposed with the other beam (named beam 2) on the adaptive

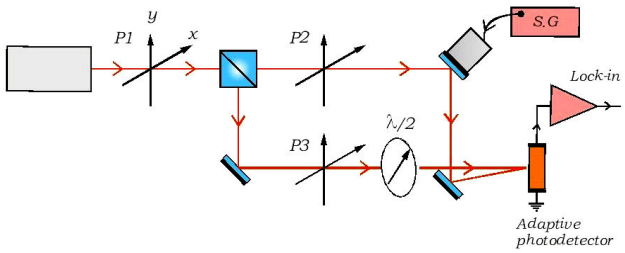

FIGURE 2.Scheme of the optical setup to verify the Fresnel and Arago interference laws by using a GaAs:Cr adaptive photodetector. S.G.: signal generator. The z-axis is along the beam propagation.

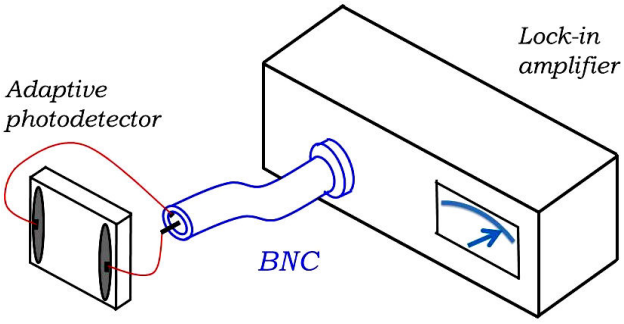

FIGURE 3. Scheme of the electrical connection of the adaptive photodetector to the lock-in amplifier. The lock-in input presents an impedance of 100 MΩ and 25 pF. BNC: 1 m BNC cable.

photodetector, forming an oscillating interference pattern, which in turn generate an alternating current through the adaptive photodetector. The electrical current generated by the photodetector is measured as a voltage drop (the p-emf signal) through the input impedance of a lock-in amplifier, which is referenced to the signal generator excitation frequency f. The use of a lock-in amplifier (Stanford Research Systems, SRS 510) allows us to measure very low level alternating electrical signals in the presence of much larger background noise; the employed lock-in amplifier presents an input impedance of 100 MΩ and 25 pF ; and a 0.5 Hz to 100 kHz frequency range. The interference angle was set at $\alpha \cong 1/75$ rad, so the period of the interference fringes was $\approx 48\ \mu$m, and the optical path difference was ≤ 8 mm, which is much lower than the coherence length of He-Ne laser employed. The excitation frequency was set at 1,600 Hz and the amplitude of vibration of the piezoelectric transducer produced an amplitude of phase modulation $A \ll 1$ rad. The time constant of the lock-in amplifier was set at 300 ms. With these settings, the noise level of the measuring system proved to be ≈ 100 nV. To verify the Fresnel and Arago interference laws the polarizers $P1$, $P2$, $P3$ and $\lambda/2$ plate were placed in the positions indicated in the same Fig. 2. A detailed scheme of the electrical connection of the adaptive photodetector to the lock-in amplifier is depicted in Fig. 3.

4. Experimental results and discussion

A simple verification of the first and second Fresnel and Arago law was carried out as follows. The polarization axis of polarizer $P1$ was set at $45°$ respect to the x-axis, so the transmitted and reflected beams by the beamsplitter had also a linear polarization at $45°$ respect to the x-axis, the polarization axes of both polarizers $P2$ and $P3$ were set at $0°$ respect to the x-axis, and the $\lambda/2$ plate was removed. As the polarization axes of the interfering beams were the same at the adaptive photodetector ($0°$ respect to the x-axis) and they were derived from the same linearly polarized wave, an oscillating interference patern with maximum visibility was expected, which in turn would generate a maximum signal from the adaptive photodetector, which

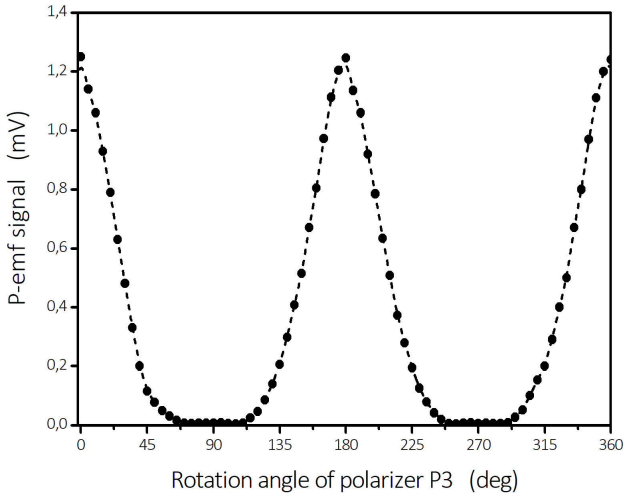

FIGURE 4. P-emf signal as a function of the rotation angle of the polarizer $P3$. The $\lambda/2$ plate was removed. Dashed line is used only to link the experimental points.

proved to be ≈ 1.25 mV in our experimental conditions; in this way, the first Fresnel and Arago law was verified.

To verify the second Fresnel and Arago law in this setup, polarizer $P3$ was rotated until its polarization axis was at $90°$ respect to the x-axis; so the linear polarization of the interfering beams were orthogonal in this case. As a result, it was expected that the interference pattern disappeared and it became a uniform light pattern, $i.e.$, a light pattern with null visibility. So, according to Eq. (1), a minimal (nominally null) p-emf signal was expected also. In our experimental conditions this minimum p-emf signal was $\approx 7\ \mu$V, which is three orders of magnitude lower than the previous case (interfering beams with parallel linear polarization).

Between these two positions of the polarizer $P3$ ($0°$ and $90°$) there is partial interference due to the polarization component of the polarizer $P3$ along the x-axis ($0°$). Because the p-emf signal is proportional to the square of the visibility of the interference pattern, the gradual change of the visibility of the interference pattern was easily observed in our experimental setup without the need for recording images and performing the corresponding image processing. The Fig. 4 shows the p-emf signal as a function of the rotation angle of polarizer $P3$ in steps of $5°$.

This Fig. 4 shows the gradual change from maximum interference (maximum p-emf signal) to null interference (minimum p-emf signal), and the corresponding polarization periodicity ($180°$). Note, however, that the light intensity of the beam 2 impinging at the adaptive photodetector is not constant; it depends on the rotation angle of polarizer $P3$, according to the Malus law. Indeed, the intensity maxima are located at $45°$ and $225°$.

To overcome the aforementioned inconvenience (nonconstant intensity of beam 2 at the adaptive photodetector) and to verify the first, second, and fourth Fresnel and Arago laws, we proceeded as follows. The polarization axis of polarizer $P1$ was set again at $45°$ respect to the x-axis, the po-

larization axes of polarizer $P2$ and $P3$ were both set again at 0° respect to the x-axis, respectively, and the $\lambda/2$ plate was inserted in the beam 2 after the polarizer $P3$, with its axis parallel to the axis of polarizer $P3$, that is at 0° respect to the x-axis. Under these initial conditions, as both of the beams were derived from the same linearly polarized beam, and they had parallel polarizations they formed an interference pattern with maximum visibility at the adaptive photodetector; which in turn generated a maximum p-emf signal. So, the first Fresnel and Arago law was verified. Note that this maximum value of the p-emf signal (≈ 0.88 mV) was lower than the maximum signal obtained in the previous case; this is due to some light absorption by the $\lambda/2$ plate, which reduced the intensity I_2 and the total light intensity I_0, see Eq. (1).

Rotation of the $\lambda/2$ plate an angle ϑ produced that the polarization axis of the emerging beam from the $\lambda/2$ plate rotated an angle 2ϑ, without changing its intensity. As a result of this rotation, the polarization axes of the interfering beams were no longer parallel, and only the component $\cos(2\vartheta)$ contributed to forming the interference pattern. Therefore, the visibility of the interference pattern decreased according to the rotation angle and as a result, the p-emf signal also diminished gradually. For a rotation angle of $\vartheta = 45^\circ$, the polarization axes of the interfering beams were orthogonal, the light pattern became uniform (*i.e.* a light pattern with zero visibility) and the p-emf signal reached its minimum value, close to the noise level. Note that even when both of the interfering beams were derived from the same linearly polarized wave, as they had orthogonal linear polarizations in this case, they did not form an interference pattern (almost zero p-emf signal); in this way, the second Fresnel and Arago law was verified.

This latter setup (two linearly polarized beams with orthogonal directions and derived from the same linearly polarized wave) was considered as the starting point to verify the fourth law. Increasing the rotation angle beyond 45°, the component $\cos(2\vartheta)$ of the polarization of beam 2 started to form an interference pattern, the visibility started to increase as well as the p-emf signal. For a rotation angle of $\vartheta = 90^\circ$ the polarization of both beams at the adaptive photodetectors were parallel again, hence both the visibility and the p-emf reached their respective maximum values.

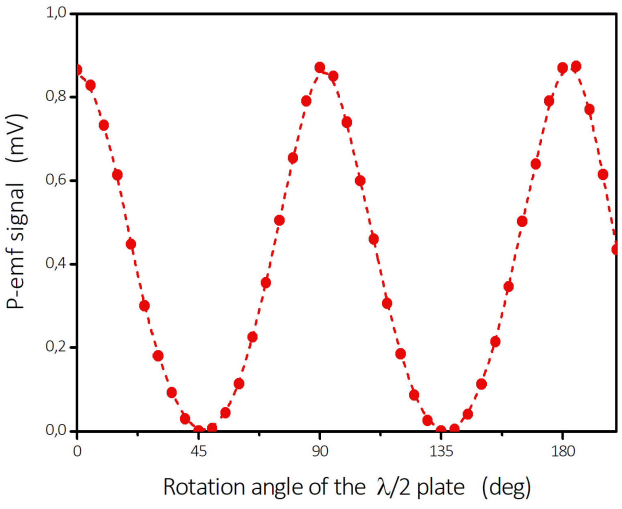

FIGURE 5. P-emf signal as a function of the rotation angle of the $\lambda/2$ plate. The polarizing axis of polarizer $P1$ was set at 45° respect to the x-axis, and the polarization axes of polarizers $P2$ and $P3$ were set at 0° respect to the x-axis. Dashed line is used only to link the experimental points.

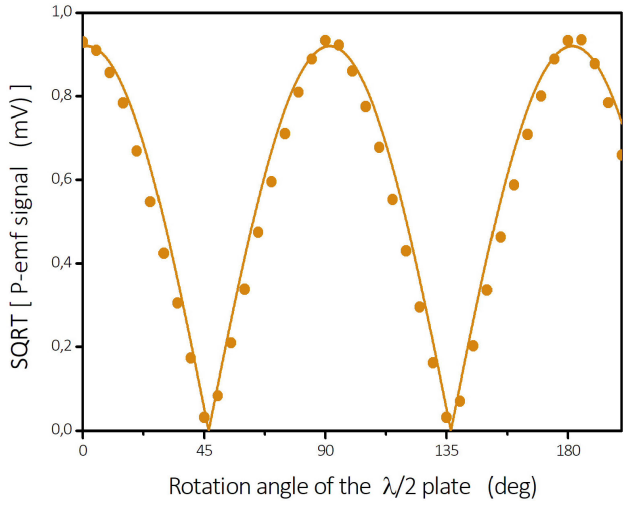

FIGURE 6. Square root of the p-emf signal values obtained from Fig. 5 as a function of the rotation angle of the $\lambda/2$ plate. Solid line is the theoretical dependence given by Eq. (3).

These features are clearly observed in Fig. 5, which shows the p-emf signal as a function of the angle of rotation of the $\lambda/2$ plate in steps of 5°. Note that the use of adaptive photodetectors allows us to locate with high accuracy the positions of maximum and minimum interference as well as observe the gradual changes between these two positions. With this procedure, the first, second, and fourth Fresnel and Arago laws were verified.

As stated in Eq. (1), the p-emf signal is proportional to the square of the Visibility of the interference pattern; so in Fig. 6 we plot the square root of the p-emf signal values (obtained from Fig. 5) as a function of the angle of rotation of the $\lambda/2$ plate.

The experimental data agree well with the theoretical dependence for the visibility, which is proportional to the absolute value of a cosine function (*i.e.* the projection of polarization axis of beam 2 to the polarization axis of beam 1). Indeed, our experimental data fit well to the following equation:

$$\text{SQRT(p-emf signal)} = 0.92\left|\cos\left(\frac{2\pi\vartheta}{180^\circ}\right)\right|, \qquad (3)$$

where ϑ is the rotation angle of the $\lambda/2$ plate. Note, however, that to measure the actual value of V and to calibrate the adaptive photodetector, it would be necessary to determine the visibility of the interference pattern according to the Michelson definition:

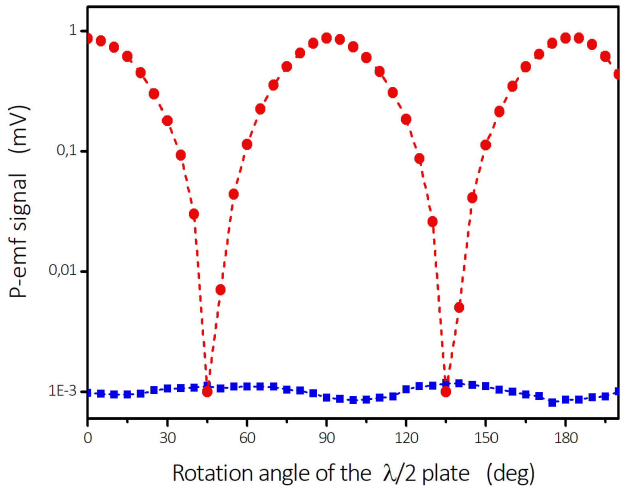

FIGURE 7. P-emf signal as a function of the rotation angle of the $\lambda/2$ plate, for two different cases: (●): beams 1 y 2 derived from the same linearly polarized wave (data taken from Fig. 5). (■): beams 1 and 2 derived from orthogonal components of the unpolarized beam.

$$V = \frac{I_{\max} - I_{\min}}{I_{\max} + I_{\min}}, \tag{4}$$

where $I_{\max}$ and $I_{\min}$ are the maximum and minimum intensities of the interference pattern, respectively.

To verify the Fresnel and Arago third law, the polarizer $P1$ was removed and, to maintain the same intensity values of the interfering beams (I_1 and I_2), a variable density filter was placed instead. The polarization axis of polarizer $P2$ was set parallel to the x-axis ($0°$) and that of polarizer $P3$ was set parallel to the $y-$axis ($90°$), that is, they were orthogonal. The axis of the $\lambda/2$ plate was set also parallel to the y-axis in this case. The signal generated by the p-emf detector was minimal. Rotating the $\lambda/2$ plate an angle of $45°$ the polarization axis of beam 2 became parallel to that of beam 1; however the p-emf signal remained practically constant, around the minimum value. This demonstrated that the beams 1 and 2 did not interfere, which was expected because they were derived from orthogonal components of unpolarized light. Hence, the third law was verified.

For comparison purposes, in Fig. 7 we plot in a semilogarithmic scale the dependencies of the p-emf signal as a function of the rotation angle of the $\lambda/2$ plate for the two experimental conditions previously described (both beams derived from the same linearly polarized wave and derived from orthogonal components of unpolarized light). The difference between the p-emf signals generated in the positions of maximum and minimum (null) interference is about 3 orders of magnitude.

Note that for the case that both beams were derived from orthogonal components of unpolarized light, it can be observed in Fig. 7 (blue squares) that the p-emf signal remains practically constant and close to the noise level, independent of the $\lambda/2$ plate rotation angle; *i.e.*, independent of the relative orientations of the interfering beams polarization axes, which indicates that in this case, the beams 1 and 2 did not interfere.

5. Conclusions

We have demonstrated the use of adaptive photodetectors experimentally in order to verify the Fresnel and Arago interference laws. As the adaptive photodetectors generate an electrical current proportional to the square of the interference pattern visibility, the gradual changes from the maximum and minimum interference positions are easily detected. These extremal positions can be assessed with high resolution, in real time, without any signal processing, and without any visual criterion. In our experimental conditions we demonstrated a difference of 3 orders of magnitude between the p-emf signals measured in the positions of maximum and minimum (null) interference.

The optical arrangement is simple and reliable. Because these adaptive photodetectors can compensate for irregularities of the interfering beams and environmental fluctuations, it is not necessary to dispose of high-quality optical elements and vibration isolation optical tables. These features allow engineering or science students to implement the experiment in an undergraduate laboratory easily. With adaptive photodetectors fabricated from GaAs or CdTe samples, the verification of the Fresnel and Arago interference laws can be carried out in the visible region of the spectrum, as well as in the near-infrared region.

1. D. F. J. Arago, and A. J. Fresnel, On the action of rays of polarized light upon each other, *Ann. Chim. Phys*. **2** (1819) 288.
2. E. Collet, *Polarized light: fundamentals and applications*, (New York, Marcel Dekker, 1993) pp 255.
3. H. J. Tiziani, N. Kerwien, and G. Pedrini, *9.1 Interferometry* in **Vol 1**: Laser Physics and Applications. Subvolume A: Laser Fundamentals. Part 2, H. Weber, G. Herziger, and R. Poprawe, Eds., (Springer-Verlag, Berlin, 2006), pp 221-284.
4. R. Hanau, Interference of linearly polarized light with perpendicular polarizations, *Am. J. Phys.* **31** (1963) 303. https://doi.org/10.1119/1.1969459
5. E. Fortin, Direct demonstration of the Fresnel-Arago law, *Am. J. Phys.* **38** (1970) 917. https://doi.org/10.1119/1.1976495
6. B. Kanseri, N. S. Biasht, S. Rath, and H. C. Kandpal, A modified version of Young's interferometer to study the Fresnel and Arago interference laws, *Eur. J. Phys*. **30** (2009) 835. https://doi.org/10.1088/0143-0807/30/4/016

7. B. Kanseri, N.S. Bisht, and H.C. Kandpal, Observation of the Fresnel and Arago laws using the Mach-Zehnder interferometer, *Am. J. Phys*. **76** (2008) 39. https//doi.org/10.1119/1.2794349
8. B. Kanseri, and H. C. Kandpal, Mathematical formulation for verification of the Fresnel and Arago interference laws using a Mach-Zehnder interferometer, *Optik* **121** (2008) 1019. https://doi.org/10.1016/j.ijleo.2008.12.003
9. M. Henry, Fresnel-Arago laws for interference in polarized light: a demonstration experiment, *Am. J. Phys*. **49** (1981) 690. https://doi.org/10.1119/1.12429
10. J.L. Ferguson, A simple, bright demonstration of the interference of polarized light, *Am. J. Phys*. **52** (1984) 1141. https://doi.org/10.1119/1.13744
11. R. Barakat, Analytic proofs of the Arago-Fresnel laws for the interference of polarized light, *J. Opt. Soc. Am. A* **10** (1993) 180. https://doi.org/10.1364/JOSAA.10.000180
12. E. Wolf, Unified theory of coherence and polarization of random electromagnetic beams, *Phys. Lett. A* **312** (2003) 263. https://doi.org/10.1016.S0375-9601(03)00684-4
13. S. Stepanov, in *Handbook of Advanced Electronic and Photonics Materials and Devices* edited by H. S. Nalwa, 2nd ed. (New York, Academic Press, 2001), p. 205.
14. M. P. Petrov, I. A. Sokolov, S. I. Stepanov, and G. S. Trofimov, Non-steady-state photo-electromotive-force induced by dynamic gratings in partially compensated photoconductors, *J. Appl. Phys*. **68** (1990) 2216. https://doi.org/10.1063/1.346525
15. P. Rodríguez Montero, C. M. Gómez-Sarabia, and J. Ojeda-Castañeda, Adaptive photodetector for assisted Talbot effect, *Appl. Opt.* **47** (2008) 3778. https://doi.org/10.1364/AO.47003778
16. E. Hecht, *Optics*, 5th ed. (London, Pearson, 2017), pp 593.
17. M. L. Arroyo Carrasco, P. Rodríguez Montero, and S. Stepanov, Measurement of the coherence length of diffusely scattered laser beams with adaptive photodetectors, *Opt. Commun.* **157** (1998) 105. https://doi.org/10.1016/S0030-4018(98)00537-9
18. S. I. Stepanov, Sensitivity of non-steady-state photoelectromotive force-based adaptive photodetectors and characterization techniques, *Appl. Opt.* **33** (1994) 915. https://doi.org/10.1364/AO.33.000915.
19. S. Stepanov, P. Rodríguez, S. Trivedi, and C. C. Wang, Effective broadband detection of nanometer laser-induced ultrasonic surface displacements by CdTe:V adaptive photoelectromotive force detector, *Appl. Phys. Lett*. **84** (2003) 446. https://doi.org/10.1063/1.1640466
20. Y. Ding, I. Lahiri, D. D. Nolte, G. J. Dunning, and D. Pepper, Electric-field correlation of femtosecond pulses by use of a photoelectromotive-force detector, *J. Opt. Soc. Am. B* **15** (1998) 2013. https://doi.org/10.1364/JOSAB.15.002013
21. C. C. Wang *et al*., Human life signs detection using high-sensitivity pulsed laser vibrometer, *IEEE Sen. J.* **7** (2007) 1370. https://doi.org/10.1109/JSEN.2007.905041